CLINICAL RESEARCH ARTICLE   OPEN

Diffuse optical tomography for the detection of perinatal stroke at the cot side: a pilot study

Maria Chalia[1], Laura A. Dempsey[2], Robert J. Cooper[2], Chuen-Wai Lee[1], Adam P. Gibson[2], Jeremy C. Hebden[2] and Topun Austin[1]

BACKGROUND: Perinatal stroke is a potentially debilitating injury, often under-diagnosed in the neonatal period. We conducted a pilot study investigating the role of the portable, non-invasive brain monitoring technique, diffuse optical tomography (DOT), as an early detection tool for infants with perinatal stroke.
METHODS: Four stroke-affected infants were scanned with a DOT system within the first 3 days of life and compared to four healthy control subjects. Spectral power, correlation, and phase lag between interhemispheric low frequency (0.0055–0.3 Hz) hemoglobin signals were assessed. Optical data analyses were conducted with and without magnetic resonance imaging (MRI)-guided stroke localization to assess the efficacy of DOT when used without stroke anatomical information.
RESULTS: Interhemispheric correlations of both oxyhemoglobin and deoxyhemoglobin concentration were significantly reduced in the stroke-affected group within the very low (0.0055–0.0095 Hz) and resting state (0.01–0.08 Hz) frequencies ($p < 0.003$). There were no interhemispheric differences for spectral power. These results were observed even without MRI stroke localization.
CONCLUSION: This suggests that DOT and correlation-based analyses in the low-frequency range can potentially aid the early detection of perinatal stroke, prior to MRI acquisition. Additional methodological advances are required to increase the sensitivity and specificity of this technique.

Pediatric Research _####################_ ; https://doi.org/10.1038/s41390-018-0263-x

INTRODUCTION

Perinatal stroke, secondary to focal disruption of cerebral arterial (perinatal arterial ischemic stroke (PAIS)) or venous (cerebral sinus venous thrombosis (CSVT)) circulation, leads to potential lifelong neurological sequelae, such as hemiparesis, epilepsy, and cognitive impairment.[1] It is the most common cause of neonatal seizures after perinatal asphyxia. Perinatal stroke may occur anywhere between the second trimester of pregnancy and the first 28 days of life.[2,3] PAIS affects up to 1 in 2300 infants,[4] with approximately 75% of cases being unilateral and involving the middle cerebral artery (MCA).[5] CSVT occurs in 2.6 in 100,000 live births.[6] Perinatal stroke is often under-diagnosed and under-reported. At present, there is no definitive treatment, other than symptomatic and supportive measures.

Magnetic resonance imaging (MRI) remains the gold standard for diagnosis of perinatal stroke,[7] but it requires transportation of infants away from the neonatal intensive care unit (NICU) and is rarely available for rapid diagnosis. Continuous wave (CW) near-infrared (NIR) diffuse optical tomography (DOT) is a safe, portable, non-invasive tool, which allows continuous brain monitoring of newborn infants at the cot side.[8] The technique measures back-scattered light from the brain and detects spatial variations in attenuation in an oxygen-dependent manner.[9] It provides information on the relative concentration changes of oxyhemoglobin (HbO$_2$) and deoxyhemoglobin (HHb), yielding total hemoglobin (HbT) when summed. DOT measures regional changes in cerebral hemodynamics associated with cortical functional activation,[10] including resting-state networks,[11] visual activation,[12] and speech development.[13] It can also detect hemodynamic changes associated with cerebral pathology.[14,15]

Diffuse optical technology has previously been employed to investigate stroke utilizing a variety of analytical approaches. For example, a decrease in the HbO$_2$ concentration ([HbO$_2$]) and increase in HHb concentration ([HHb]) (i.e., reduced oxygen saturation) during focal cerebral ischemia has been observed in rats,[16,17] piglets,[18] and adult human patients undergoing neurovascular surgery who suffered an ischemic event.[19] Vernieri et al. demonstrated abnormal changes in the cerebral blood volume of stroke-affected tissue following a hypercapnic challenge in two adults with unilateral MCA stroke.[20] Cooper et al. used a CW-DOT and electroencephalography (EEG) system to identify successive large changes in both [HbO$_2$] and [HbT] that were significantly different between the healthy and stroke-affected brain regions of a term infant with extensive unilateral stroke.[21] While these studies provide valuable insight, transient hemodynamic changes are not always observed in stroke-affected infants, and it is not possible to subject them to hypercapnia. Additionally, commercial NIR technologies that can measure quantitative variables like tissue oxygen saturation tend to provide limited spatial sampling.

We investigated the utility of CW-DOT for early detection of perinatal stroke by studying interhemispheric patterns in these spontaneous low-frequency oscillations (LFOs). LFOs are believed to be associated with myogenic,[22] metabolic,[23]

[1]Neonatal Intensive Care Unit, The Rosie Hospital, Cambridge University Hospitals NHS Foundation Trust, Cambridge CB2 0QQ, UK and [2]Department of Medical Physics and Biomedical Engineering, University College London, Gower Street, London WC1E 6BT, UK
Correspondence: Topun Austin (topun.austin@addenbrookes.nhs.uk)
These authors contributed equally: Maria Chalia, Laura A. Dempsey.

Diffuse optical tomography for the detection of perinatal stroke at the...
M Chalia et al.

2
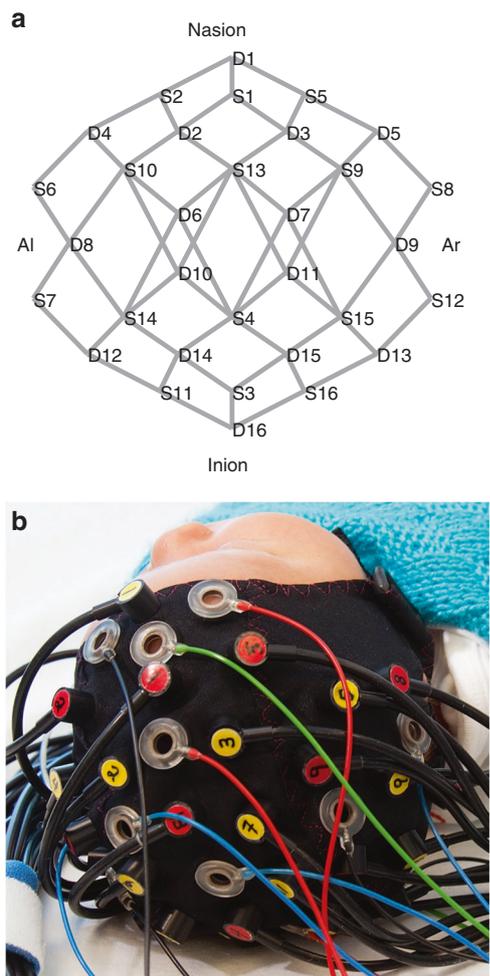
Fig. 1 The diffuse optical tomography array. **a** Source (S) and detector (D) placement yields 58 channels (indicated in gray). **b** Cap being worn by an infant. The cap can also incorporate electro-encephalography electrodes if seizure monitoring is desired. Al preauricular left, Ar preauricular right

neurogenic stimuli,[24] sympathetic tone,[25] and cerebral auto-regulation.[26,27] LFOs were subdivided into the bands of very low (VL; ~0.007 Hz),[28] resting state (RS; ~0.04 Hz),[29] and Mayer waves (~0.1 Hz).[30] White et al. obtained CW-DOT data from the visual cortex of one infant with unilateral occipital stroke and demonstrated disrupted interhemispheric correlation of [HbO$_2$] signals at frequencies below respiration.[11] To our knowledge, we are the first group to apply LFO analysis to whole-head CW-DOT data from stroke-affected infants. We hypothesized that a detectable difference in LFO content would exist between the stroke-affected and healthy hemispheres of infants with perinatal stroke. To test the efficacy of CW-DOT used in isolation within the first few days of life, we performed our analysis both with and without MRI-guided stroke localization.

METHODS
Study approval was obtained by the National Research Ethics Service Committee, East of England (REC Reference 09/H0308/125, IRAS project ID: 24005). The data that support the findings of this study are available from the corresponding author upon reasonable request.

Subjects
Following informed parental consent, infants were recruited upon their admission to the NICU at the Rosie Hospital, Cambridge. Control infants were scanned within the first 2 days of life (except for CTRL_3 who was scanned 19 days after birth, near term-equivalent age) and had no confounding conditions. Infants presenting with focal seizures and clinical suspicion of stroke were scanned within the first 3 days of life. An MRI (as per standard clinical care) confirmed the diagnosis of stroke between 7 and 10 days of life.

Data acquisition
A 16-source and 16-detector CW-DOT device (NTS, Gowerlabs Ltd., London, UK) with a sampling frequency of 10 Hz was used for data acquisition. The measurement obtained by a single source-detector pair is referred to as a "channel." The scanning protocol, source-detector array (Fig. 1a), and cap (Fig. 1b) are described in more detail in our previously published work.[14,15] Healthy infants are generally more difficult to scan with DOT due to increased levels of movement, leading to shorter scan times. This contrasts with sick infants, who are often sedated and therefore remain relatively still throughout long periods of data recording.
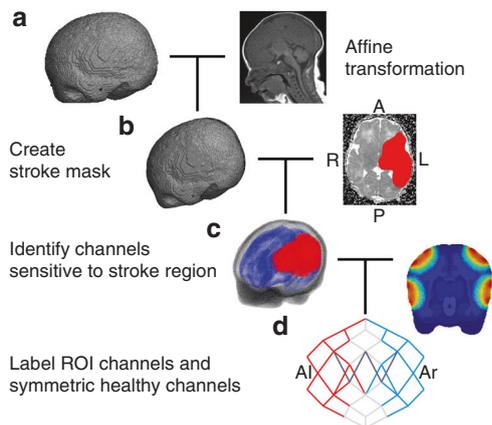
MRI processing
The anatomical landmarks of nasion, inion, preauricular right (Ar), preauricular left (Al), and central zero (Cz) were measured using the T1 spin echo (SE) MRI of each stroke-affected infant (FSL).[31] To accommodate the range of head shapes across the stroke cohort (Fig. 2a), an age-matched neonatal head atlas mesh[32] was affine transformed to each infant's anatomical landmarks (Fig. 3a). The stroke-affected region was marked by a consultant neonatologist in each infant's MRI (Fig. 2b) and used to create a volumetric mask of the stroke-affected tissue in the subject's affine-transformed mesh (Fig. 3b). For practical reasons, the MRI sequence that most clearly showed the stroke area was used to create the mask. In ascending order from Stroke_1 to Stroke_4, the MRI sequence used was T1-SE, T2 fast spin echo (FSE), T2-FSE, and apparent diffusion coefficient. Although the authors acknowledge that different sequences may highlight tissue damage to varying extents, it was assumed to a first approximation that visible stroke volume remained consistent across sequences. To identify which channels sampled stroke-affected tissue, simulations of light propagation through the brain were created by applying the finite element method to the affine-transformed meshes (TOAST++,[33] see previous work for more details[14,15]). The simulations yielded a photon measurement density function (PMDF) for each channel, which represented how sensitive a single DOT measurement was to the underlying tissue. Each PMDF was thresholded at 10% of its maximum sensitivity and included in a region of interest (ROI) if it overlapped with the volumetric stroke mask (Fig. 3d, red lines).

Optical data pre-processing
All data were processed in MATLAB (R2012b, MathWorks, Natick, MA). The data were pre-processed by removing channels containing poor quality data according to three criteria: (1) Channels with a mean measured intensity below the noise floor of the device (corresponding to 10^{-4} au as recommended by the manufacturer) were rejected. (2) Channels with a signal-to-noise ratio (SNR) < 5 were removed (this threshold was chosen by inspection). (3) Channels displaying motion artifact were rejected first using an automatic detection algorithm implemented in the HOMER2 plugin (www.homer-fnirs.org) and second using manual rejection following inspection. The remaining data segments were realigned along the mean of the data and concatenated (Fig. 4a). Intensity data were converted to optical density and then to [HbO$_2$] and [HHb] using the modified Beer–Lambert Law and a differential pathlength factor of 4.[34] The hemoglobin concentration data

Diffuse optical tomography for the detection of perinatal stroke at the…
M Chalia et al.

3
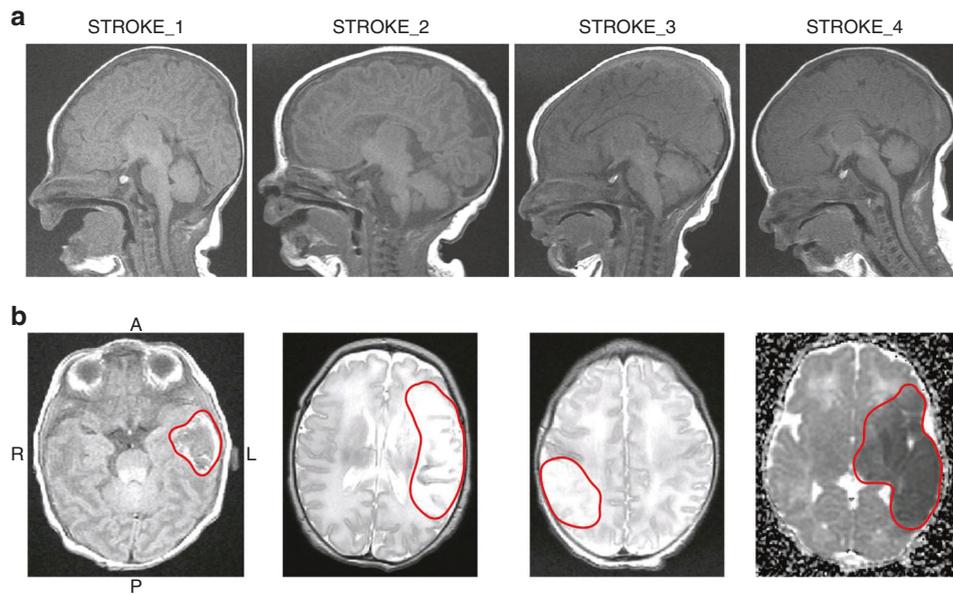
Fig. 2 Magnetic resonance images (MRIs). **a** Sagittal T1 spin echo (SE) views of each stroke-affected infant's head, demonstrating the large variety in head shapes. **b** Axial slices showing abnormal signal in the stroke region (red line). A anterior, P posterior, R right, L left. The MRI sequence from left to right is T1-SE, T2 fast spin echo (FSE), T2-FSE, and apparent diffusion coefficient (ADC)

Fig. 3 Data, mesh, and magnetic resonance image pre-processing. **a** The age-matched atlas mesh is affine transformed to the infant's head coordinates; **b** the infant's stroke mask is created and combined with the affine-transformed mesh to determine the region of interest (ROI); **c** the labeled mesh is combined with a light simulation to determine **d**, which channels overlap by at least 10% with the stroke ROI (red). The symmetric healthy channels are subsequently identified (blue) and channels with a signal-to-noise ratio <5 are excluded (dark gray). Representative examples of steps **a**–**d** are shown for Stroke_4. A anterior, P posterior, R right, L left
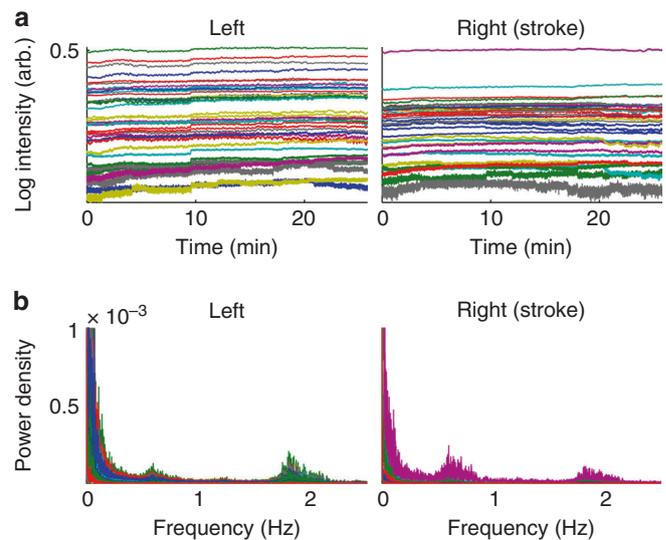
Fig. 4 Representative examples of diffuse optical tomography data from Stroke_3. **a** Concatenated log intensity data from all channels with signal-to-noise ratio >5. **b** Power spectral density of the stroke-blind channels and symmetric healthy channels

were bandpass filtered into the VL (0.0055-0.0095 Hz), RS (0.01–0.08 Hz), and Mayer wave (0.09–0.3 Hz) bands, guided by inspection of the data spectral power (Fig. 4b). The low pass filter was a third-order Butterworth filter, and the high pass filter was a fifth-order Butterworth filter. Every infant's data length satisfied the Nyquist criterion for the slowest investigated frequency (0.0055 Hz) and were within limits for LFO analysis.[35]

"Blind channels" were defined as all channels covering the same hemisphere as the stroke. "ROI channels" were defined for each stroke-affected infant as those that had PMDFs overlapping with the volumetric stroke mask (Fig. 3c, d, red lines). For both groups, the healthy symmetric channels (Fig. 3d, blue lines) were used for interhemispheric LFO comparisons. Channels (and their symmetric partners) with insufficient SNR were excluded from analysis. For the control cohort, channels located over the left hemisphere were treated as blind channels.

Analysis and statistics
Power spectral density (PSD) was calculated for the [HbO$_2$] and [HHb] signals and integrated within the three LFO bands. The Wilcoxon signed-rank test was used to assess interhemispheric differences in spectral power for each subject. Test results were corrected for multiple comparisons by dividing the original 1% threshold for significance by the number of frequency bands, i.e., $0.01/3 = 0.0033 = p_\alpha$.

4

Pearson's *R* and the maximum phase lag (seconds) between every symmetric channel pair within each LFO band were calculated for both the [HbO$_2$] and [HHb] signals. Using Fisher's Z-Transformation, the correlation *R*-values were converted to Z-scores. Anderson–Darling test showed that the Z-scores for each infant did not form a normal distribution at a significance level of 5%; therefore, non-parametric tests were employed for subsequent analysis. To identify any significant differences in interhemispheric correlation and phase lag between the control and stroke-affected infants, the data were grouped into three cohorts: the stroke-blind, stroke-ROI, and control group. Mann–Whitney *U* test was used to compare each stroke-related group to the control group. The Z-score results were converted back to *R*-values for visualization. The significance threshold was set as before to $p_\alpha = 0.0033$.

RESULTS

Clinical details

Between December 2014 and August 2016, 11 infants presented with seizures and a clinical suspicion of stroke; 8 were consented. Of these 8 infants, 4 were included in the analysis. Among the excluded four subjects, only one was proven to have stroke but the quality of the data was poor. Out of the remaining three, one had MRI findings consistent with hypoxic ischemic encephalopathy, and the other two had a normal MRI with no identifiable cerebral injury at the time. Ten controls were recruited, four of which were included in the analysis based on data quality. Clinical details of the infants analyzed are summarized in Table 1.

Stroke_1 presented with dusky, cyanotic spells. As other clinical causes were excluded, and these events persisted, the infant received a loading dose of Phenobarbitone (20 mg/kg) 9 h prior to data acquisition and no further anticonvulsant treatment. Stroke_2 presented with decerebrate posturing and hypotonia at the background of prolonged labor and profound anemia at birth. Electrical seizures were noted during data acquisition (on amplitude integrated EEG—as part of standard clinical monitoring). A loading dose of Phenobarbitone (20 mg/kg) was given at the end of the study (this was a clinical decision independent to the conduction of the study). Stroke_3 presented with tonic movements of all four limbs at the local hospital for which the infant received Phenobarbitone, Phenytoin, and Clonazepam. No further seizures were noted after transfer to the tertiary center and the infant was scanned 3 days after receipt of anticonvulsant treatment. Stroke_4 presented with clonic movements of the right lower limb during an infection screen at the local hospital, for which a loading dose of Phenobarbitone (20 mg/kg) was given. No further seizure activity was noted after transfer to the tertiary center and the infant was scanned 3 days later.

Optical data

Approximately 80% of channels were included in the analysis for each infant, the remainder being rejected owing to poor SNR. Figure 4a shows an example of the concatenated optical intensity signal for Stroke_3. Cardiac and respiratory oscillations are apparent at approximately 1.9 and 0.6 Hz in the Fourier transform of the signal (Fig. 4b). The length of the data was on average 27 min (range 22 min) for each stroke-affected infant and 12 min (range 13.7 min) for each control infant.

Spectral power content

There was no significant difference in interhemispheric spectral power content in the control or stroke-affected cohort, except for Stroke_2. For Stroke_2, the spectral power of the [HbO$_2$] and [HHb] signals was significantly less in the healthy hemisphere compared to the stroke-affected hemisphere in all LFO bands.

Correlation

Figure 5 depicts the interhemispheric correlation results for the control group alongside the stroke blind and ROI groups. The central mark of the box is the median. The bottom and top edges are the 25th and 75th percentiles, respectively. The whiskers extend to the most extreme points not identified as outliers. A statistically significant difference in interhemispheric correlation ($p_\alpha < 0.0033$) within the VL and RS bands for both [HbO$_2$] and [HHb] was observed between the control group and both the stroke-blind and stroke-ROI groups. There was a significant difference between the stroke-ROI group and control group for the [HHb] signal in the Mayer wave band (Fig. 5b).

Phase lag

The phase lag analysis did not return any statistically significant results, regardless of whether blind or ROI channels were investigated. The stroke-affected hemisphere [HbO$_2$] oscillations preceded the healthy hemisphere by a median 2.5 s in the VL frequency band for the stroke-blind group ($p_\alpha = 0.079$) and 3.3 s for the stroke-ROI group ($p_\alpha = 0.052$), but p_α was insufficient in both instances and hence results were not interpreted further. A trend was observed in the interquartile range (IQR) of the [HbO$_2$] VL signal across the groups. The IQRs for the stroke-ROI, stroke-blind, and control groups were 144.0, 39.9, and 9.2 s, respectively. Compared to the control group, the VL IQR increase was 1565% for the stroke-ROI group and 434% for the stroke-blind group.

DISCUSSION

Our results showed a significant difference in interhemispheric correlation between the control group and stroke-affected groups within the VL and RS bands, with the stroke-blind group showing an approximate 30–50% decrease in correlation for both [HbO$_2$] and [HHb]. No significant difference was found in interhemispheric LFO spectral power in either the control or stroke-affected infants (apart from Stroke_2, discussed below) or in interhemispheric phase lag. However, the IQR of the phase lag within the VL band was markedly increased in the stroke-affected patients compared to the controls, particularly when the analysis was limited to the stroke ROI.

Our hypothesis was that stroke-affected regions would have altered vascular tone with a marked impact on the LFO content of the DOT signal. This was based on results suggesting interhemispheric difference in spectral power that have been published from a single stroke-affected infant scanned at 10 weeks of life.[11] A possible explanation for the lack of spectral power results could be that stroke-affected infants were scanned early, prior to bulk tissue necrosis, thereby making any underlying spectral power change undetectable. Li et al. studied spontaneous left prefrontal cerebral oscillations among adults at risk for atherosclerotic stroke with single-channel NIR spectroscopy. They performed a wavelet transform analysis in five subdivided frequency bands (0.005–2.0 Hz), and observed significantly lower spectral power for [HHb] and [HbO$_2$] in the at-risk cohort.[36] Perhaps the primarily different pathophysiological cascade in this instance compared to perinatal stroke may also explain why we did not see any difference in spectral frequency band power. The one exception was subject Stroke_2, who had lower [HbO$_2$] and [HHb] spectral power within the healthy hemisphere compared to the stroke-affected hemisphere. This discrepancy was attributed to ongoing seizure activity. The continuous amplitude-integrated EEG during the scan showed five discrete epileptiform episodes arising from the stroke-affected side, which could explain the observed interhemispheric difference in spectral power content. The remaining stroke-affected infants did not have seizure activity immediately before or during data acquisition. Additionally, these infants received anticonvulsant treatment for a significant period of

Diffuse optical tomography for the detection of perinatal stroke at the…
M Chalia et al.

5

Table 1. Subject information

Subject ID	GA (weeks)	CGA at scan (weeks)	Respiratory	Neurology	Diagnosis/MRI findings	DOT channels incl. (%)
Stroke_1	38 + 4	38 + 6	HFNC	Apneas, Seizures	Perinatal stroke. Large hemorrhagic lesion in the left temporal lobe associated with overlying subdural hemorrhage; secondary to venous infarction	82.76
Stroke_2	37 + 2	37 + 3	SIMV+VG	Seizures	Left MCA infarct, HIE II. Abnormal signal intensities within the territory of the left MCA consistent with infarction. Involvement of the basal ganglia, thalami, and PLIC on the left with abnormal diffusion in the Left cerebral peduncle	79.31
Stroke_3	40	40 + 3	SVIA	Seizures	Right MCA infarct. Large infarct over the right hemisphere, involving the temporal, parietal, and occipital lobe	79.31
Stroke_4	41 + 3	41 + 6	SVIA	Seizures	Left MCA infarct. Abnormal signal intensity within white matter, cortex, and basal ganglia within the territory of the left MCA consistent with infarction	89.66
CTRL_1	37 + 5	38	SVIA	Normal	Healthy, no MRI	72.41
CTRL_2	40 + 1	40 + 2	SVIA	Normal	Healthy, no MRI	93.10
CTRL_3	31 + 5	34 + 3	SVIA	Normal	Healthy, no MRI	48.28
CTRL_4	37 + 2	37 + 3	SVIA	Normal	Healthy, no MRI	93.10

Clinical details of the stroke-affected and control infants (CTRL)
CGA corrected gestational age, DOT diffuse optical tomography, GA gestational age, HFNC high flow nasal cannula, HIE hypoxic ischemic encephalopathy, MCA middle cerebral artery, MRI magnetic resonance imaging, PLIC posterior limb of the internal capsule, SIMV+VG synchronized intermittent mandatory ventilation with volume guarantee, SVIA self-ventilating in air
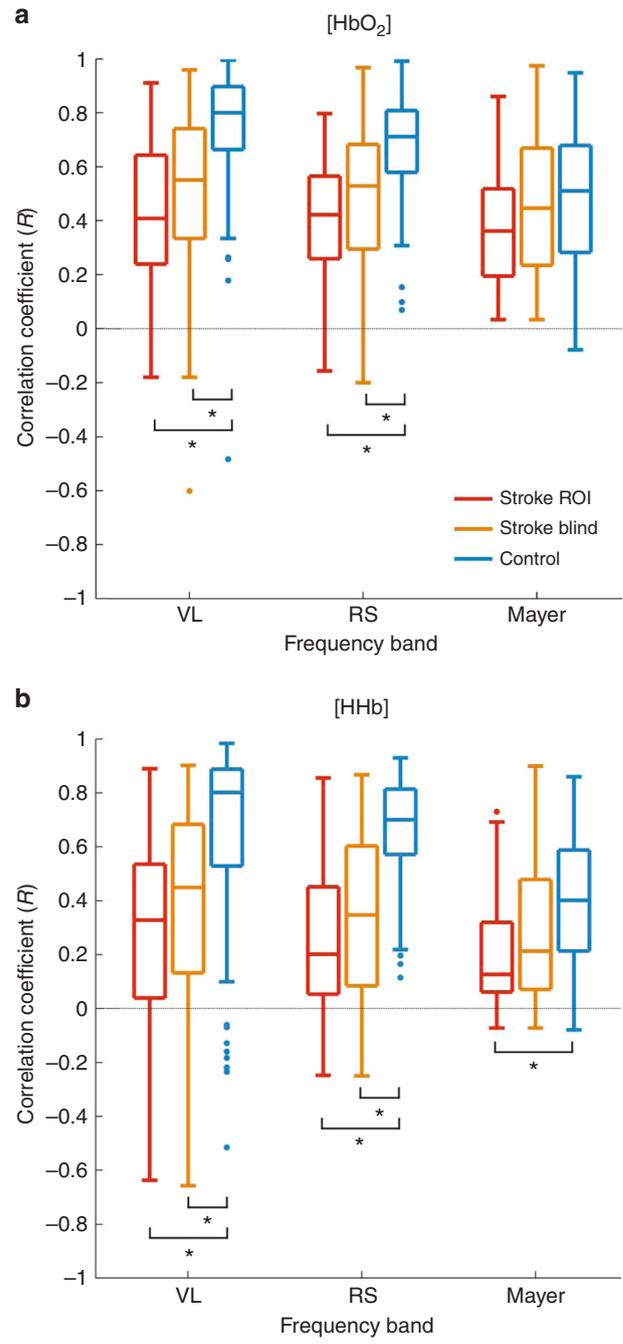
Fig. 5 Correlation results between symmetric pairs of stroke-region of interest (ROI) channels (red), stroke-blind channels (orange), and control channels (blue) in each frequency band for oxygenated hemoglobin concentration ([HbO$_2$]) (**a**) and deoxygenated hemoglobin concentration ([HHb]) (**b**). Statistical significance is denoted by *$p < 0.0033$. VL very low, RS resting state

time before data acquisition and hence there should be no pharmacological impact on the DOT signal.

The dramatic drop in interhemispheric correlation in the stroke-affected group was the most striking result of this study. The correlation results for the stroke-blind channels were highly significant and only slightly less than those of the stroke-ROI channels. This demonstrates that MRI is not a prerequisite for optical signal analysis, thus reinforcing the potential value of DOT

Diffuse optical tomography for the detection of perinatal stroke at the...
M Chalia et al.

6

as an early diagnostic tool. Mirroring these correlation results, White et al. observed interhemispheric correlation values of approximately 0.8 for $[HbO_2]$ and 0.65 for $[HHb]$ in healthy control infants, whereas an infant with occipital stroke had markedly decreased correlation of 0.2 for $[HbO_2]$ and -0.15 for $[HHb]$.[11] Their device covered only the occipital cortex with 106 channels, whereas our array consists of 58 channels covering the entire head. The sparse and global arrangement of our array potentially "dilutes" the effect of the damaged brain tissue on the interhemispheric correlation results but offers the ability to detect stroke over the entire superficial cortical surface. Experimental DOT images of cortical activation that parallel the spatial resolution and accuracy of functional MRI have recently been reported,[37] but currently available commercial systems have insufficient channel count to replicate these results. We expect the tradeoff between field of view and spatial resolution to diminish as novel DOT systems become high density, modular, lightweight, and wireless.[38]

The results from the interhemispheric phase lag analysis were not significant. Changes in $[HbO_2]$ within the VL band in the stroke-affected hemisphere always preceded those of the healthy hemisphere for both the stroke-blind and stroke-ROI channels, but these results should be interpreted with caution given the insufficient p_α. An increasing variability was noted in the VL band $[HbO_2]$ phase lag values as sensitivity to the stroke region improved. In comparison to the control group, the IQR increase was qualitatively apparent (434%) for the stroke-blind group and almost four times that (1565%) for the stroke-ROI group. This result warrants further investigation, as it supports the idea that absolute interhemispheric phase shift (as opposed to defining a leading or lagging relationship between signals) may be a more valuable metric. For example, Phillip et al. showed that the absolute interhemispheric phase shift between low-frequency arterial blood pressure (ABP) and cerebral $[HbO_2]$ oscillations was significantly less in patients undergoing thrombolytic therapy compared to untreated stroke adults.[39] Han et al. found a significantly lower-phase coherence within the lower-frequency bands in hypertensive elderly patients with cerebral infarction.[40] These studies demonstrated a disruption to absolute interhemispheric phase patterns within the VL and RS frequency bands in stroke-affected adults, adding credence to the idea that physical injury to the MCA affects VL and RS oscillations, and that these frequency bands should be a target of investigation for stroke detection.

Statistically significant results in the Mayer wave band were only observed in the interhemispheric spectral power of Stroke_2 and in the $[HHb]$ correlation results between the control group and stroke-ROI group. Mayer waves have been detected in several species at different inherent frequencies and present at 0.1 Hz in humans.[41] Studies suggest that Mayer waves are global oscillations in ABP correlating with sympathetic neuronal activity,[30] that they trigger the release of endothelial-derived nitric oxide during vascular stress,[42] or that they are part of normal vascular baroreflex mechanisms and of no particular function.[43] A possible explanation for the lack of results obtained in this band could be that these oscillations are transient phenomena which exist independently alongside hemodynamic events rather than in response to hemodynamic changes.[30] In conjunction with the fact that other oscillations (RS, respiration) exist near the frequency of 0.1 Hz,[44] it becomes difficult to attribute any specific physiological meaning to the $[HHb]$ correlation result obtained. However, our results support growing evidence that inclusion of Mayer wave frequencies in LFO analysis can obscure meaningful results in the RS band.[44]

A limitation of this study is the lack of other physiological parameters acquired that could be correlated to the cerebral DOT signal. For example, continuous ABP was not recorded as it was not clinically indicated. This study is also limited by the small number of subjects identified over the project's duration. However, this was a single-center study run over a 20-month period. With an incidence of perinatal stroke of 1 in 2300 live births,[4] and approximately 5500 deliveries per year at the Rosie Hospital, Cambridge, this was a foreseeable limitation. However, these results demonstrate the ability of DOT to diagnose neonatal stroke at the cot side and could form the basis for a larger multicenter study.

Summary
To our knowledge, this is the first study using a multichannel, whole-head DOT system to evaluate perinatal stroke in the acute phase. Our results align with previous evidence of disrupted low-frequency interhemispheric brain function in stroke-affected patients. The interhemispheric correlation results warrant further development of the technique, especially considering that their diagnostic capability does not require MRI. These findings could serve as the basis of a larger study that establishes DOT as an early, cot-side, diagnostic tool for perinatal stroke, which would complement existing neuro-monitoring and neuro-imaging methodologies to inform clinical management and prognosis. This could potentially facilitate the study of early treatment strategies for perinatal stroke, such as therapeutic hypothermia.[45]

AUTHOR CONTRIBUTIONS
M.C., R.J.C., J.C.H., A.P.G. and T.A. conceived the study. L.A.D. and C.-W.L. designed the cap and array. L.A.D., M.C. and C.-W.L. collected the control data. M.C. collected the stroke data and M.C. performed the pre-processing. L.A.D. performed the analysis. M.C. and L.A.D. drafted the article, and all authors contributed substantially to its revision. M.C., L.A.D., C.-W.L., R.J.C. and T.A. made substantial contributions to conception and design, acquisition of data, or analysis and interpretation of data. M.C., L.A.D., R.J.C., A.P.G., J.C.H. and T.A. were responsible for drafting the article or revising it critically for important intellectual content. T.A. gave final approval of the version to be published.

ADDITIONAL INFORMATION
Competing interests: R.J.C. has financial interests in the UCL spin-out company, Gowerlabs Ltd., which did not influence this work. The other authors declare no competing interests.

Publisher's note: Springer Nature remains neutral with regard to jurisdictional claims in published maps and institutional affiliations.

REFERENCES
1. Golomb, M. R. Outcomes of perinatal arterial ischemic stroke and cerebral sinovenous thrombosis. *Semin Fetal Neonatal Med.* **14**, 318–322 (2009).
2. Lynch, J. K. & Nelson, K. B. Epidemiology of perinatal stroke. *Curr. Opin. Pediatr.* **13**, 499–505 (2001).
3. Raju, T. N., Nelson, K. B., Ferriero, D., Lynch, J. K. & NICHS-NINDS Perinatal Stroke Workshop Participants. Ischemic perinatal stroke: summary of a workshop sponsored by the National Institute of Child Health and Human Development and the National Institute of Neurological Disorders and Stroke. *Pediatrics* **120**, 609–616 (2007).
4. Wu, Y. W., Lynch, J. K. & Nelson, K. B. Perinatal arterial stroke: understanding mechanisms and outcomes. *Semin Neurol.* **25**, 424–434 (2005).
5. Volpe, J. J. in *Neurology of the Newborn* 5th edn 379–388 (Saunders, Philadelphia, 2008).
6. Ramenghi, L. A., Govaert, P., Fumagalli, M., Bassi, L. & Mosca, F. Neonatal cerebral sinovenous thrombosis. *Semin Fetal Neonatal Med.* **14**, 278–283 (2009).
7. Lequin, M. H., Dudink, J., Tong, K. A. & Obenaus, A. Magnetic resonance imaging in neonatal stroke. *Semin Fetal Neonatal Med.* **14**, 299–310 (2009).

Diffuse optical tomography for the detection of perinatal stroke at the…
M Chalia et al.

7

8. Lee, C. W., Cooper, R. J. & Austin, T. Diffuse optical tomography to investigate the newborn brain. *Pediatr. Res.* **82**, 376–386 (2017).

9. Scholkmann, F. et al. A review on continuous wave functional near-infrared spectroscopy and imaging instrumentation and methodology. *Neuroimage* **85**(Pt 1), 6–27 (2014).

10. Chance, B. et al. A novel method for fast imaging of brain function, non-invasively, with light. *Opt. Express* **2**, 411–423 (1998).

11. White, B. R., Liao, S. M., Ferradal, S. L., Inder, T. E. & Culver, J. P. Bedside optical imaging of occipital resting-state functional connectivity in neonates. *Neuroimage* **59**, 2529–2538 (2012).

12. Liao, S. M. et al. High-density diffuse optical tomography of term infant visual cortex in the nursery. *J. Biomed. Opt.* **17**, 081414 (2012).

13. Sato, H. et al. Cerebral hemodynamics in newborn infants exposed to speech sounds: a whole-head optical topography study. *Hum. Brain Mapp.* **33**, 2092–2103 (2012).

14. Singh, H. et al. Mapping cortical haemodynamics during neonatal seizures using diffuse optical tomography: a case study. *Neuroimage Clin.* **5**, 256–265 (2014).

15. Chalia, M. et al. Hemodynamic response to burst-suppressed and discontinuous electroencephalography activity in infants with hypoxic ischemic encephalopathy. *Neurophotonics* **3**, 031408 (2016).

16. Wolf, T. et al. Noninvasive near infrared spectroscopy monitoring of regional cerebral blood oxygenation changes during peri-infarct depolarizations in focal cerebral ischemia in the rat. *J. Cereb. Blood Flow. Metab.* **17**, 950–954 (1997).

17. Culver, J. P. et al. Three-dimensional diffuse optical tomography in the parallel plane transmission geometry: evaluation of a hybrid frequency domain/continuous wave clinical system for breast imaging. *Med. Phys.* **30**, 235–247 (2003).

18. Stankovic, M. R. et al. Real-time optical imaging of experimental brain ischemia and hemorrhage in neonatal piglets. *J. Perinat. Med.* **27**, 279–286 (1999).

19. Calderon-Arnulphi, M. et al. Detection of cerebral ischemia in neurovascular surgery using quantitative frequency-domain near-infrared spectroscopy. *J. Neurosurg.* **106**, 283–290 (2007).

20. Vernieri, F. et al. Near infrared spectroscopy and transcranial Doppler in mono-hemispheric stroke. *Eur. Neurol.* **41**, 159–162 (1999).

21. Cooper, R. J. et al. Transient haemodynamic events in neurologically compromised infants: a simultaneous EEG and diffuse optical imaging study. *Neuroimage* **55**, 1610–1616 (2011).

22. Auer, L. M. & Gallhofer, B. Rhythmic activity of cat pial vessels in vivo. *Eur. Neurol.* **20**, 448–468 (1981).

23. Hudetz, A. G., Smith, J. J., Lee, J. G., Bosnjak, Z. J. & Kampine, J. P. Modification of cerebral laser-Doppler flow oscillations by halothane, PCO2, and nitric oxide synthase blockade. *Am. J. Physiol.* **269**(1 Pt 2), H114–H120 (1995).

24. Mayhew, J. E. et al. Cerebral vasomotion: a 0.1-Hz oscillation in reflected light imaging of neural activity. *Neuroimage* **4**(3 Pt 1), 183–193 (1996).

25. Tachtsidis, I. et al. Investigation of cerebral haemodynamics by near-infrared spectroscopy in young healthy volunteers reveals posture-dependent spontaneous oscillations. *Physiol. Meas.* **25**, 437–445 (2004).

26. Schytz, H. W. et al. Spontaneous low-frequency oscillations in cerebral vessels: applications in carotid artery disease and ischemic stroke. *J. Stroke Cerebrovasc. Dis.* **19**, 465–474 (2010).

27. Kuo, T. B., Chern, C. M., Sheng, W. Y., Wong, W. J. & Hu, H. H. Frequency domain analysis of cerebral blood flow velocity and its correlation with arterial blood pressure. *J. Cereb. Blood Flow. Metab.* **18**, 311–318 (1998).

28. Kvandal, P. et al. Low-frequency oscillations of the laser Doppler perfusion signal in human skin. *Microvasc. Res* **72**, 120–127 (2006).

29. Biswal, B. B., Van Kylen, J. & Hyde, J. S. Simultaneous assessment of flow and BOLD signals in resting-state functional connectivity maps. *NMR Biomed.* **10**, 165–170 (1997).

30. Julien, C. The enigma of Mayer waves: Facts and models. *Cardiovasc Res.* **70**, 12–21 (2006).

31. Smith, S. M. et al. Advances in functional and structural MR image analysis and implementation as FSL. *Neuroimage* **23**(Suppl 1), S208–S219 (2004).

32. Brigadoi, S., Aljabar, P., Kuklisova-Murgasova, M., Arridge, S. R. & Cooper, R. J. A 4D neonatal head model for diffuse optical imaging of pre-term to term infants. *Neuroimage* **100**, 385–394 (2014).

33. Schweiger, M. & Arridge, S. The Toast++ software suite for forward and inverse modeling in optical tomography. *J. Biomed. Opt.* **19**, 040801 (2014).

34. Arri, S. J., Muehlemann, T., Biallas, M., Bucher, H. U. & Wolf, M. Precision of cerebral oxygenation and hemoglobin concentration measurements in neonates measured by near-infrared spectroscopy. *J. Biomed. Opt.* **16**, 047005 (2011).

35. Wang, J., Dong, Q. & Niu, H. The minimum resting-state fNIRS imaging duration for accurate and stable mapping of brain connectivity network in children. *Sci. Rep.* **7**, 6461 (2017).

36. Li, Z. et al. Spectral analysis of near-infrared spectroscopy signals measured from prefrontal lobe in subjects at risk for stroke. *Med. Phys.* **39**, 2179–2185 (2012).

37. Eggebrecht, A. T. et al. Mapping distributed brain function and networks with diffuse optical tomography. *Nat. Photonics* **8**, 448–454 (2014).

38. Chitnis, D. et al. Functional imaging of the human brain using a modular, fibreless, high-density diffuse optical tomography system. *Biomed. Opt. Express* **7**, 4275–4288 (2016).

39. Phillip, D. et al. Spontaneous low frequency oscillations in acute ischemic stroke – a near infrared spectroscopy (NIRS) study. *J. Neurol. Neurophysiol.* **5**, 1000241 (2014).

40. Han, Q. et al. Phase synchronization analysis of prefrontal tissue oxyhemoglobin oscillations in elderly subjects with cerebral infarction. *Med. Phys.* **41**, 102702 (2014).

41. Cooke, W. H. et al. Human responses to upright tilt: a window on central autonomic integration. *J. Physiol.* **517**(Pt 2), 617–628 (1999).

42. Nafz, B. et al. Antihypertensive effect of 0.1-Hz blood pressure oscillations to the kidney. *Circulation* **101**, 553–557 (2000).

43. Chapuis, B., Vidal-Petiot, E., Orea, V., Barres, C. & Julien, C. Linear modelling analysis of baroreflex control of arterial pressure variability in rats. *J. Physiol.* **559** (Pt 2), 639–649 (2004).

44. Bumstead, J. R., Bauer, A. Q., Wright, P. W. & Culver, J. P. Cerebral functional connectivity and Mayer waves in mice: phenomena and separability. *J. Cereb. Blood Flow. Metab.* **37**, 471–484 (2017).

45. Wu, T. C. & Grotta, J. C. Hypothermia for acute ischaemic stroke. *Lancet Neurol.* **12**, 275–284 (2013).